Entropy and bifurcations in a chaotic laser

Pieter Collins*
Department of Mathematical Sciences, University of Liverpool, Liverpool L69 7ZL, United Kingdom

Bernd Krauskopf†
Department of Engineering Mathematics, University of Bristol, Bristol BS8 1TR, United Kingdom
(Received 21 March 2002; published 7 November 2002)

We compute bounds on the topological entropy associated with a chaotic attractor of a semiconductor laser with optical injection. We consider the Poincaré return map to a fixed plane, and are able to compute the stable and unstable manifolds of periodic points globally, even though it is impossible to find a plane on which the Poincaré map is globally smoothly defined. In this way, we obtain the information that forms the input of the entropy calculations, and characterize the boundary crisis in which the chaotic attractor is destroyed. This boundary crisis involves a periodic point with negative eigenvalues, and the entropy associated with the chaotic attractor persists in a chaotic saddle after the bifurcation.

DOI: 10.1103/PhysRevE.66.056201 PACS number(s): 05.45.−a, 95.10.Fh, 42.55.Px

I. INTRODUCTION

Many physical systems exhibit low-dimensional chaotic dynamics. Well-known examples include the Lorenz system [1] and various forced nonlinear oscillators; see Ref. [2] and further references therein. How can one show that a given system is chaotic, or better, determine how chaotic it is? Established methods are the computation of Lyapunov exponents [3] and estimating the fractal dimension of a chaotic attractor [4]. Both methods are computationally expensive and may be inaccurate.

An alternative approach is to compute symbolic dynamics relative to a partition of phase space. The symbolic dynamics of the Hénon map was described by finding the pruning fronts [5], using approximate homoclinic tangencies to attempt to construct a generating partition [6–8]. However, while this approach appears to yield good results in practice, only heuristic arguments are given as to why the computed dynamics should indeed occur in the system under consideration. [In Ref. [7] the authors remark that the method ''appears to be of general validity, although there is no rigorous proof that it is always applicable.''] The dynamics associated with so-called single-sided homoclinic tangles was studied in Ref. [9], but again the results are mathematically nonrigorous. More recently, some mathematically rigorous techniques of constructing symbolic dynamics have emerged, such as topological approximation theory [10] and Conley index methods [11,12].

In this paper, we use the trellis theory developed in Refs. [13,14]. In this method, the symbolic dynamics is computed by a mathematically rigorous construction from a knowledge of finite pieces of stable and unstable manifolds of saddle points of the system. Since these manifolds can be computed arbitrarily accurately, the method is a computationally feasible approach to the construction of symbolic dynamics. The method has the additional advantages of describing the dynamics in terms of the natural partition of phase space by the computed manifolds, and of giving the existence of periodic, homoclinic and heteroclinic orbits. As far as we are aware, no other method for computing symbolic dynamics shares all these useful properties. While the aim is not necessarily to construct a generating partition as in Ref. [8], we can find the dynamics arbitrarily precisely by computing arbitrarily long pieces of manifold. We believe that combining the two methods may give an even more powerful approach to computing symbolic dynamics, but this is beyond the scope of the paper.

We can use the symbolic information obtained from the trellis theory to find a lower bound for the topological entropy [15]. Topological entropy is a single number measuring how chaotic a given system is, much like a Lyapunov exponent. [There is indeed a deep mathematical connection between the two concepts [16].] While Lyapunov exponents measure how chaotic an individual attractor is, topological entropy is a *global measure* of chaos, and is associated with homoclinic and heteroclinic tangles formed by the stable and unstable manifolds of saddle periodic orbits. For low-dimensional systems, the topological entropy measures the growth rate of the number of hyperbolic periodic orbits, another natural measure of the complexity of the system; see Ref. [17] for a method to estimate this growth rate.

To showcase the power of our method for practical applications we consider the technologically relevant example of a semiconductor laser subject to external optical injection, introduced in Sec. II below. It is known that optical injection produces an enormous variety of different dynamics, including chaos [18–23], and it was recently considered for chaotic communication schemes [24,25]. Its bifurcation (or stability) diagram has been studied extensively [22] and excellent agreement was found with experimental measurements [21,26]. This revealed different routes to regions of chaos in the system, and sudden bifurcations of chaotic attractors [27,28].

In this paper, we consider one such transition, in which a chaotic attractor is seen to disappear. This phenomenon is caused by a boundary crisis, which is a bifurcation in which

*Electronic address: pcollins@liv.ac.uk
†Electronic address: B.Krauskopf@bristol.ac.uk

a chaotic attractor is destroyed when it collides with its basin boundary. Boundary crises have been extensively studied [29–31], and are especially well understood when they occur at a homoclinic or heteroclinic tangency of stable and unstable manifolds [32]. Here we discuss the boundary crisis in terms of the unstable manifold of a saddle fixed point in the chaotic attractor. Because the stable eigenvalue of this saddle point is negative, the boundary crisis is not due to a tangency involving this unstable manifold, but instead occurs at the first intersection of its *closure* and the *closure* of the stable manifold of a different saddle point. We therefore call this type of boundary crisis a *closure tangency*. A closure tangency was noted by Osinga and Feudel in their paper Ref. [33] on quasiperiodically forced systems when they looked at the (unforced) orientation-reversing Hénon map. Here we give the first detailed account of this type of boundary crisis in the orientation-preserving case, which is especially important since this is the case which occurs in the Poincaré map of a flow. The disappearance of the chaotic attractor also raises the interesting question of what happens to the entropy during the bifurcation.

Our main tool is to consider a Poincaré or first return map to a suitable section (i.e., a smooth codimension-one manifold). For the much-studied periodically forced systems, the stroboscopic map of the forcing frequency is a Poincaré map with the extra property that the plane of fixed forcing transversely intersects *all* orbits of the vector field (in autonomous form). Therefore, this Poincaré map is a *globally defined* diffeomorphism; for example, for the forced Van der Pol and Duffing oscillators [2] it is a globally defined planar map. However, it is an important fact that this is a special property of periodically forced systems. For a general flow it is not possible to find a section that is transverse to all orbits [34]. This means that one is condemned to work with a section on which the Poincaré first return map need not be invertible, may have discontinuities and may even be (locally) undefined. This must be seen as the typical situation in applications and is also the case for the laser system considered here. As a consequence, one encounters new features in the organization of the stable and unstable manifolds that do not occur in the more familiar case of surface diffeomorphisms such as the Hénon [35] and Ikeda [36] maps. We stress that the difficulties caused by the discontinuities in the first Poincaré return map *cannot* be circumvented by a clever choice of section.

Adapting the method in Ref. [37] to this more general setting allows us to compute suitably long pieces of stable and unstable manifolds. These are the input to the topological algorithm of Ref. [13] by which we establish rigorous bounds for the topological entropy. This constitutes a proof that the semiconductor laser with optical injection does indeed have chaotic dynamics.

This paper is organized as follows. In Sec. II we introduce the equations of an optically injected semiconductor laser and discuss its Poincaré map. Global bifurcations are explained in detail in Sec. III and the entropy bounds are the topic of Sec. IV. We draw some conclusions and point to future work in Sec. V. The Appendix is a brief exposition in the Hénon map of a boundary crisis at a closure tangency.

II. SEMICONDUCTOR LASER WITH OPTICAL INJECTION

A semiconductor laser with optical injection is arguably the most accessible laser system showing chaotic dynamics, being modeled very well by the single-mode rate equations

$$\dot{E} = K + \left(\frac{1}{2}(1+i\alpha)n - i\omega\right)E, \tag{1}$$

$$\dot{n} = -2\Gamma n - (1+2Bn)(|E|^2 - 1),$$

for the complex electric field E and the population inversion n [22]. The main parameters are the injected field strength K and the detuning ω of the injected field from the solitary laser frequency. The parameters α, B, and Γ specify material properties of the laser. In particular, α is the well-known linewidth enhancement factor and for semiconductor lasers it is in the range $\alpha \in [1,10]$. In this paper, we set the material laser parameters to the realistic values $\alpha = 2$, $B = 0.015$, and $\Gamma = 0.035$; see Ref. [22] for further details.

A. The Poincaré map

To study system (1), we consider the first Poincaré return map f to a section. This has the advantage of reducing the system to a two-dimensional iterated map, which is easier to visualize and is more amenable to many kinds of analysis. It is usual to consider a Poincaré section which is everywhere transverse to the flow and to which all trajectories return, in which case the resulting map is globally defined, continuous and invertible. Unfortunately, for the semiconductor laser, there is no such global section, so instead we take a natural section Σ for the system, namely the plane $\Sigma = \{(E,n) : n = 0\}$, and treat the resulting pathologies appropriately.

If p_0 is a point on Σ such that the trajectory through p_0 has a first return to Σ at a point p_1, and the flow is transverse to Σ at p_0 and p_1, then the first return map f is locally a diffeomorphism at p_0. On these regions, f can be treated like any other diffeomorphism and no special theory is required. However, some initial conditions p_0 may lie in the basin of an attractor which does not intersect Σ. Indeed, it may even be that the trajectory through p_0 never returns to Σ. In this case, the first return map is undefined at p_0. For initial conditions approaching the boundary of the domain of definition of f, the return time typically tends to infinity.

Another serious problem is that the first return map f need not be continuous. In all cases, a discontinuity of the return map is due to a loss of transversality of the flow with the section. Before discussing the various cases, we first examine the behavior of the flow of system (1) on Σ.

Since Σ is defined by the condition $n = 0$, the direction in which the flow crosses Σ is given by the sign of $\dot{n}$ at $n = 0$. From Eq. (1) we see that

$$\dot{n}|_{n=0} = 1 - |E|^2, \tag{2}$$

so n increases through Σ when $|E| < 1$ and decreases when $|E| > 1$. The flow is tangent to Σ precisely on the unit circle C given by $|E| = 1$. For this system, the tangency set is in-

dependent of the parameter values. Even though this parameter independence is not typical, we note that the tangency set is one dimensional, which is the generic case.

On C we compute

$$\frac{d}{dt}(|E|^2) = 2K\mathrm{Re}(E), \tag{3}$$

so the flow is directed toward the outside of C for $\mathrm{Re}(E) > 0$ and inside for $\mathrm{Re}(E) < 0$.

Locally, C divides Σ into two pieces, Σ_1 and Σ_2, which we can choose so that the vector field is directed from Σ_1 to Σ_2. Assuming further the generic case of a quadratic tangency, we see that points in Σ_1 return to the section in Σ_2 after a time interval which tends to 0 as the starting point approaches C, whereas points in Σ_2 have no local returns to Σ. Therefore, C is a discontinuity curve of f, with $f(p) \approx p$ if p is in Σ_1 and close to C, but typically $f(p) \notin C$ for $p \in C$.

Despite these discontinuities, the first return map is still invertible, since an inverse is given by reversing the flow direction. There are three generic types of discontinuity, corresponding to a flow line which is tangent to the section Σ at an initial, interior or final point, respectively. In two of these cases, a locally continuous map can be constructed by allowing the number of returns to the section to vary.

The easiest situation is that the tangency occurs at an interior point of the flow line joining two points. Changing the number of intersections with the section by two allows a smooth extension of the return map, as the flow is transverse to the section at the initial and final points. Similarly, when the tangency occurs at the initial point of the flow line, changing the number of intersections with the section by one allows a continuous extension of the return map, though this is not smooth. However, when the tangency occurs at the final point of the flow line, there is no continuous extension. It is possible to change the number of intersections by one and obtain a return map which is close to the original one.

A continuous extension of the return map is known as a *branch* of the return map. These branches are best understood by considering the set

$$\{(p_0, p_1, t) \in \Sigma \times \Sigma \times \mathbf{R} : \Phi_t(p_0) = p_1\},$$

which gives all possible returns. A more detailed discussion of nonglobally defined Poincaré maps, which must be regarded typical in applications, is beyond the scope of this paper.

B. Stable and unstable manifolds

A great deal of information about the dynamics of the system can be obtained by computing the stable and unstable manifolds of its periodic saddle orbits. For the laser system (1), with parameter values $K = 0.290$ and $\omega = 0.270$, we consider two periodic saddle orbits P and Q, with periods 13.14 and 13.19, respectively. The stable and unstable eigenvalues of P are both positive, and those of Q are negative, so the invariant manifolds of Q are nonorientable [38]. We call P a *direct* saddle orbit and Q a *flip* (or *twisted*) saddle. The product of stable and unstable eigenvalues for both P and Q is less than 1, so both saddles are *dissipative*, that is, the attracting direction is stronger than the repelling one.

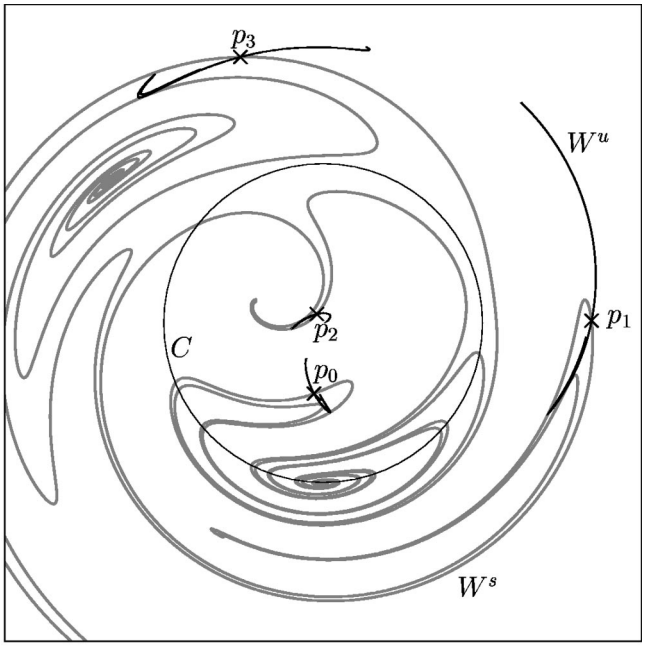

FIG. 1. Stable and unstable manifolds of the four-periodic points $\{p_0, p_1, p_2, p_3\}$, which are in the same orbit under the Poincaré map f, shown in the section $\{n = 0\}$ in this and all other figures; $\omega = 0.270$ and $K = 0.290$. On the circle $C = \{|E| = 1\}$ the Poincaré map is discontinuous.

Both of these orbits cross the section Σ at four points, which are, therefore, four-periodic points of the first return map f. We label these point p_0, p_1, p_2, p_3 and q_0, q_1, q_2, q_3, where the convention is that the points map to each other in this order and back to p_0 or q_0, respectively. Figure 1 shows the stable and unstable manifolds of the orbit $P = \{p_0, p_1, p_2, p_3\}$.

The stable and unstable manifolds of the p_i, denoted $W^s(p_i)$ and $W^u(p_i)$, respectively, consist of the intersection of the stable and unstable manifolds of P with the section Σ. Since the stable manifold of P is a smooth surface, its intersection with any section will (generically) consist of an immersed collection of one-dimensional manifolds. However, the presence of discontinuities in the first return map means that the properties of the stable manifold may be very different from that of the stable manifold of a surface diffeomorphism. Indeed, we can see that the stable manifolds through p_0 and p_3 and those through p_1 and p_2 coincide. This would be impossible for a diffeomorphism, but can occur here as the stable curve passes through the tangency curve C. In addition, there are components of the stable manifold which do not contain any of the points p_0, p_1, p_2, p_3.

The presence of discontinuities complicates the computation of the invariant manifolds. Most algorithms for computing one-dimensional invariant manifolds involve computing the invariant manifold in a neighborhood of the periodic orbit and growing it. Here we use an adaptation of the algorithm of Krauskopf and Osinga [37], which we combine with the observation that the computation of a continuous branch

of the return map can be formulated as a family of boundary value problems. In this way, stable and unstable manifolds can be continued across discontinuities of the first return map by changing the number of iterates. At present we compute the return map by shooting, but one could also use collocation techniques in combination with standard continuation methods, such as is done in the package AUTO [39].

III. GLOBAL BIFURCATIONS

We now consider the bifurcations of the system as the parameter ω is increased from 0.260 to 0.280 keeping K fixed at 0.290. In this region, sudden bifurcations to chaos have been found in numerically computed bifurcation diagrams [23], and later also in an experiment on an optically injected distributed feedback (DFB) laser [26]. Here we consider this transition in much more detail, and this requires looking in a small range for ω. The periodic saddle orbits P and Q which were computed for $\omega=0.270$ can be continued through this parameter range, and they remain direct and flip saddles, respectively.

In this ω range we encounter two important bifurcations contributing to the disappearance of a chaotic (strange) attractor A, which is present for $\omega=0.26$. The first bifurcation we encounter is a *basin boundary metamorphosis* [31] at $\omega=\omega_{\mathrm{bbm}}\approx 0.269\,292$, followed by a *boundary crisis* [29] at $\omega=\omega_{\mathrm{bc}}\approx 0.269\,299$. The basin boundary metamorphosis is due to an *inner tangency* [32] of the stable and unstable manifolds of the direct saddle P. At this well-known bifurcation the attractor A itself does not change, but the basin boundary undergoes a smooth to fractal transition (as was observed, for example, in the Hénon map [31]) due to the creation of a chaotic saddle. The boundary crisis is caused by a *closure tangency*: the first intersection of the closure of $W^u(Q)$, which constitutes the attractor A, and the closure of $W^s(P)$, which contains the boundary of the basin of attraction. In fact, because Q is a flip saddle, there cannot be a parameter value at which a first tangency of $W^s(P)$ and $W^u(Q)$ exists. After the boundary crisis the system jumps to a periodic attractor.

A closure tangency has not been described in detail. It was discussed briefly in Ref. [33] in the orientation-reversing case. In the Appendix we illustrate this global bifurcation and, in particular, the organization of $W^u(Q)$, in the orientation-preserving Hénon map.

The inner tangency removes a topological obstruction for the boundary crisis to occur. It is not unusual for a basin boundary metamorphosis to be followed closely by a boundary crisis. This occurs, for example, in the vicinity of a double crisis point; see Ref. [40]. However, entropy considerations show that it is impossible for a first inner tangency to occur simultaneously with a boundary crisis of a chaotic attractor, so a double crisis is not responsible for the closeness of these two bifurcations in our system. Instead, our investigations suggest that the closeness is due to the fact that the stable eigenvalue of P is very small (≈ 0.03 over the entire range $\omega\in[0.260,0.280]$).

A description of the bifurcations can be obtained by considering the Poincaré return map to Σ. As ω varies, P and Q each continue to intersect Σ transversely at four points. The chaotic attractor A intersects Σ in four components, A_0,A_1,A_2,A_3, with each A_i containing q_i and being invariant under f^4. The component A_0 is contained in the rectangle $R=[-0.1,-0.2]\times[-0.65,0.35]$. Although f, and hence f^4 are not globally continuous, the restriction of f^4 to R is, so the dynamics on this set is essentially that of a diffeomorphism, and is governed by the two periodic saddle points p_0 and q_0 and their stable and unstable manifolds.

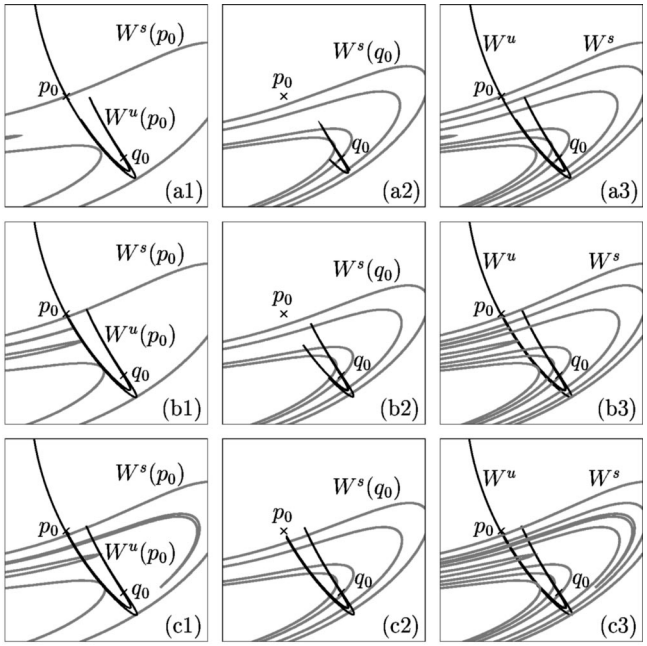

FIG. 2. Stable and unstable manifolds of the four-periodic point p_0 (left column), of the four-periodic point q_0 (middle column), and of both p_0 and q_0 (right column), before (row a), approximately at (row b) and after (row c) the destruction of a chaotic attractor; $K=0.290$ and from (a) to (c) ω=0.2673, 0.269292, 0.270.

A. Basin boundary metamorphosis at inner tangency

For parameter values of ω less than ω_{bbm}, the geometry of the stable and unstable manifolds of p_0 and q_0 is as shown in Fig. 2 (row a). The closure of the unstable manifold of the flip saddle q_0 is a chaotic attractor A_0 with a positive Lyapunov exponent and positive entropy. For many parameter values, this attractor may have smaller subattractors inside it, including stable periodic orbits [41], but the observable behavior is that of a single strange attractor. One branch of the unstable manifold of p_0 ends in a periodic attractor r_0, and the other branch intersects the stable manifold of q_0. Hence, points near p_0 are either attracted to A_0 or to r_0. The stable manifold of p_0 does not intersect the unstable manifold of p_0, so there are no orbits homoclinic to p_0.

The stable and unstable manifolds to p_0 at the inner tangency bifurcation occurring for $\omega=\omega_{\mathrm{bbm}}$, are shown in Fig. 2(b1). The attractor A_0 persists, but there is now a new basic set associated with the homoclinic orbits to p_0, also with positive topological entropy. This leads to a change of the

basin of A_0, and this is why this inner tangency is in fact a basin boundary metamorphosis. Since the direct saddle p_0 is dissipative, a result of Palis and Takens [42] shows that there must have been chaotic attractors present near p_0 even before this bifurcation, but these are small enough not to be physically relevant. The significance of this bifurcation is that now there are no topological obstructions for the stable manifold of p_0 to intersect the unstable manifold of q_0.

B. Boundary crisis at closure heteroclinic tangency

The attractor A is destroyed in the boundary crisis occurring at $\omega=\omega_{\rm bc}$, soon after the inner tangency. For $\omega<\omega_{\rm bc}$, the stable manifold of p_0, $W^s(p_0)$, and the unstable manifold of q_0, $W^u(q_0)$, are disjoint, and we have a chaotic attractor consisting of the closure of the unstable manifold of q_0, $\overline{W^u(q_0)}$. For $\omega>\omega_{\rm bc}$, the manifolds $W^s(p_0)$ and $W^u(q_0)$ intersect transversely, and we now have a heteroclinic tangle formed by the stable and unstable manifolds of p_0 and q_0. Therefore $\overline{W^u(q_0)}$ and $\overline{W^u(p_0)}$ are the same, and the closure of the unstable manifold $W^u(q_0)$ is no longer a chaotic attractor. Instead, almost every point is attracted to the periodic point r_0. This bifurcation gives a *discontinuous* change in the closure of $W^u(q_0)$.

As ω approaches $\omega_{\rm bc}$ from above, there are infinitely many parameter values at which heteroclinic tangencies of $W^s(p_0)$ and $W^u(q_0)$ occur, and $\omega_{\rm bc}$ is a limit point of these values. Since q_0 is a flip saddle, its unstable manifold limits on itself from both sides, so it can never have tangencies with any stable manifold without also having transverse crossings. At $\omega_{\rm bc}$, the manifolds $W^s(p_0)$ and $W^u(q_0)$ must still be disjoint, but they do have common limit points. Therefore, the closures of the manifolds, $\overline{W^s(p_0)}$ and $\overline{W^u(q_0)}$, intersect, and numerical evidence strongly suggests that $\overline{W^s(p_0)}$ and $\overline{W^u(q_0)}$ are smoothly tangent at the bifurcation, justifying the name *closure tangency*. Although $W^s(p_0)$ and $W^u(q_0)$ are disjoint, there may be periodic saddle points in $\overline{W^s(p_0)}$ and $\overline{W^u(q_0)}$ whose unstable manifolds do have a first tangency at $\omega_{\rm bc}$, in which case the crisis is as described in Ref. [29].

The closure tangency can be seen as a bifurcation of the chaotic saddle B associated with the homoclinic tangle of P and the attractor A associated with the homoclinic tangle of Q; see the Appendix. A natural consequence is that at the bifurcation, the topological entropy associated with A and B must be the same; see also Sec. IV.

IV. TOPOLOGICAL ENTROPY

As mentioned in the introduction, topological entropy is a global measure of the degree of chaos of a dynamical system, and is associated with the growth rate of the number of periodic points of a given period. There is also a notion of entropy applied to a homoclinic or heteroclinic tangle, which is given in terms of the growth rate of the number of intersections of initial branches of stable and unstable manifold under iteration of the latter. The entropy of a tangle is equal to the growth rate of the periodic orbits associated with the tangle. Since some entropy may be associated with other tangles of the system, the entropy of the tangle under consideration is a lower bound for the topological entropy of the system.

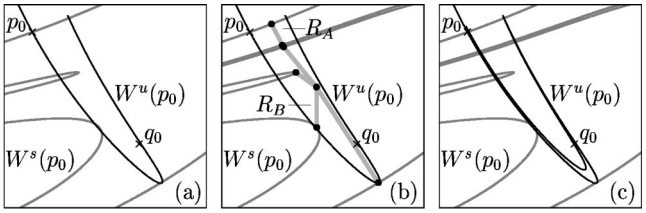

FIG. 3. Initial branches of stable and unstable manifolds of p_0 from Fig. 2 form a trellis that does not force chaotic dynamics (a). For a longer piece of $W^s(p)$ the trellis bounds two regions R_A and R_B with positive entropy dynamics (b), while an even longer piece of $W^s(p)$ reveals that the regions of chaotic dynamics are thin strips (c); $K=0.290$ and $\omega=0.270$.

Here, we estimate the topological entropy of the fourth return map of the semiconductor laser using the methods described in Refs. [13,14] and also give a detailed description of the system in terms of symbolic dynamics. For the remainder of this section, we shall use $\tilde{f}$ to refer to the fourth return map f^4 of the laser system.

The quality of the information obtained depends greatly upon the length of stable and the unstable manifolds one computes. Consider the initial pieces of stable and unstable manifold, called a *trellis*, shown in Fig. 3(a). The stable and unstable manifolds are such that no information about the entropy can be obtained other than the standard result that it must be strictly positive.

In Fig. 3(b), the trellis divides Σ into a number of regions. It can be shown that the regions R_A and R_B must contain chaotic dynamics. Orbits that are entirely contained in these two regions can be coded symbolically by assigning to each orbit the sequence of A's and B's such that the kth element of the sequence gives the region containing the kth iterate. Such a sequence is called an *itinerary* of the point. Using our methods, we can show that $\tilde{f}$ must have orbits of every itinerary except those which contain a word of the form $AB^{4n+k}A$ where $k=1$ or $k=2$; see below for more details.

Increasing the length of computed stable and unstable manifolds allows better estimates of the symbolic dynamics, and better entropy bounds can be obtained. The unstable curve shown in Fig. 3(c) is the iterate of that shown in Fig. 3(b). We can now deduce that the chaotic saddle, which must exist in regions R_A and R_B, must lie in the very thin strip bounded by the indicated piece of $W^u(p_0)$.

We now return to consider the trellis for $\omega=0.270$ of Fig. 3(b) in more detail. The symbolic dynamics is found by constructing a graph G embedded in the complement of the unstable manifold, and using the stable manifold to induce an action g on this graph; see Fig. 4. The edges of G are of two types, *control edges*, shown in black, and *expanding edges*, shown in gray. The control edges are short edges crossing the stable manifold. Their primary role is to capture the topological and dynamical information contained in the stable manifold. The expanding edges connect the control edges without crossing the trellis or introducing unnecessary loops. They

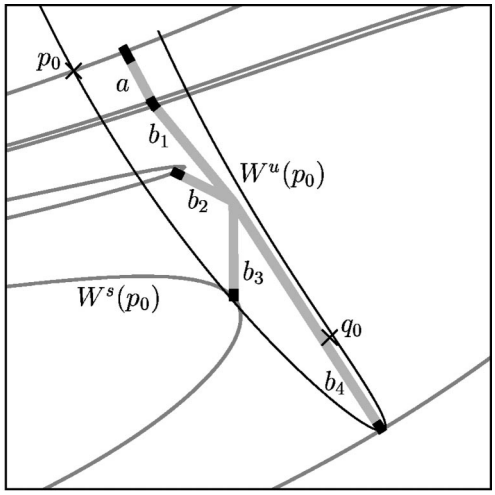

FIG. 4. Initial branches of stable and unstable manifolds of p_0 from Fig. 3(b), with a corresponding graph G capturing the topology of the trellis; $K=0.290$ and $\omega=0.270$.

carry all the interesting dynamical information.

Performing the algorithm given in Ref. [13] we obtained the graph in Fig. 4. The induced action g on the expanding edges of the graph is given by

$$a \mapsto a b_1 \overline{b_2},\ b_1 \mapsto b_2,\ b_2 \mapsto b_3,\ b_3 \mapsto b_4,\ b_4 \mapsto a b_1. \quad (4)$$

We see that orbits of g also have an itinerary given by A's and B's, with the edge a corresponding to A, and the edges b_1, b_2, b_3, and b_4 corresponding to B.

The most important property of g is that for any orbit of g, there is an orbit of $\tilde{f}$ with the same itinerary. The orbits of g are said to *force* orbits of $\tilde{f}$. Furthermore, for any periodic orbit of g, there is a periodic orbit of $\tilde{f}$ with the same itinerary and period. For example, the four-periodic orbit of g that visits edges a, b_2, b_3, and b_4 forces a four-periodic orbit of $\tilde{f}$ with itinerary $(ABBB)^{\mathbf{Z}}$. We can also deduce information about the orbits of $\tilde{f}$ that are homoclinic to p_0: for any orbit of g that has all but finitely many points in a (and so whose itinerary is homoclinic to $A^{\mathbf{Z}}$), there is a corresponding orbit of $\tilde{f}$ which is homoclinic to p_0.

The converse of these forcing results is not true; the orbits of $\tilde{f}$ do not force orbits of g, and in many cases there *must* be orbits of $\tilde{f}$ that have a different itinerary from any orbit of g. Therefore, all we can say is that the dynamics of $\tilde{f}$ are more complicated than those of g. This is well reflected in the topological entropy, which satisfies the inequality

$$h_{top}(\tilde{f}) \geq h_{top}(g). \quad (5)$$

For this example of $\omega=0.270$, we find $h_{top}(g)\approx\ln(1.544)\approx 0.434$, giving a lower bound for the entropy of the system as $h_{top}(f^4)\geq 0.434$. This proves that the injection laser as modeled by Eq. (1) indeed has chaotic dynamics (for these particular parameter values).

TABLE I. Lower estimates of the topological entropy of $\tilde{f}=f^4$, $K=0.290$, and ω is as indicated.

ω	$\omega_{\mathrm{bc}}\approx 0.269292$	0.278	0.280	0.282
$h_{top}(\tilde{f})$	0.436	0.596	0.596	$\ln 2\approx 0.693$

We now study how the topological entropy changes with the parameter ω; the resulting estimates for the entropy are summarized in Table I. For $\omega<\omega_{\mathrm{bc}}$, the topological entropy of the attractor A_0 can be estimated by considering the trellis formed by the stable and unstable manifolds of q_0. Since the stable manifold of p_0 and the unstable manifold of q_0 do not intersect, the dynamics on the attractor can be considered separately from that of the chaotic saddle associated with p_0. For the stable and unstable manifolds of q_0 computed for both $\omega=\omega_{\mathrm{bbm}}$ and $\omega=\omega_{\mathrm{bc}}$, the bound for the entropy of the attractor is 0.346, though the actual entropy may increase slightly. At $\omega=\omega_{\mathrm{bbm}}$, the entropy of the trellis associated with p_0 is 0, and at the closure tangency, the entropy of the trellises associated with p_0 and q_0 must be equal, hence the entropy of the trellis associated with p_0 must be at least 0.346.

As ω increases further, more intersections of stable and unstable manifold are created. While some of the fine structure of the tangle may change for ω between 0,272 and 0.280, there are no significant changes. For ω between 0.280 and 0.282, there is a bifurcation sequence, illustrated in Fig. 5, which ends in the creation of a full Smale horseshoe. The entropy bound for the chaotic saddle increases, and appears to change continuously with ω, though the bound computed from given finite pieces of stable and unstable manifold jumps at the homoclinic tangencies. For the trellises in Fig. 5, we compute entropy bounds of 0.596, 0.596, and $\ln 2\approx 0.693$, respectively; see also Table I. However, this entropy only measures the complexity of the transient orbits, and would not be seen if the system was already locked to the stable limit cycle r_0; see Sec. II. It is a curious phenomenon that the entropy of the chaotic set is increasing as ω increases past the closure tangency. In other words, while the *complexity* of the system as measured by the topological entropy is increasing, the *observed* behavior becomes simpler, because the chaotic set loses stability and only r_0 remains as an attractor.

V. CONCLUSIONS

The method of analysis presented here can be extended to any low-dimensional system. We have seen that invariant

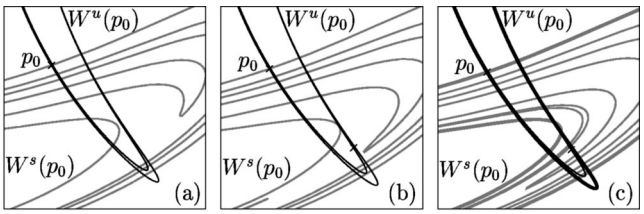

FIG. 5. The emergence of a full horseshoe of f^4; $K=0.290$ and from (a) to (c) $\omega=0.278$, 0.280, 0.282.

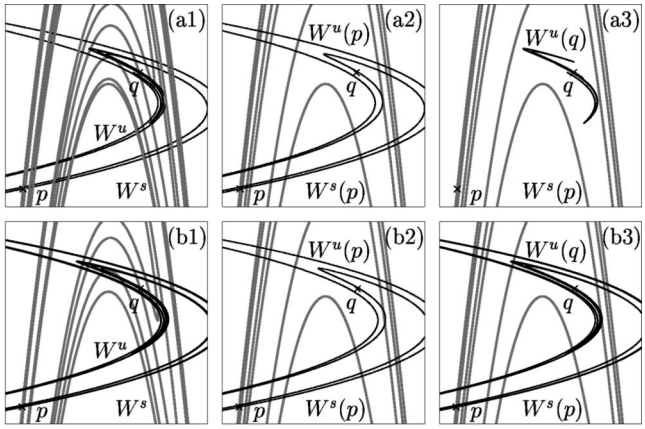

FIG. 6. Before (row a) and after (row b) a closure tangency in the Hénon map. Shown are the stable and unstable manifolds of p and q (left column), just of p (middle column), and the stable manifold of p and unstable manifold of q (right column); $b=0.5$, and $a=2.4$ (row a) and $a=2.5$ (row b).

curves of saddle points in a section can be computed even if there is no globally defined, continuous, invertible first return map (which is the typical situation). From these manifolds, the structure of the large-scale attractors of the system can be computed, and bifurcations in which they are destroyed can also be found.

One can then compute rigorous lower bounds for the topological entropy on attractors and chaotic nonattracting sets, and obtain a description of their internal dynamics in terms of the itineraries.

For the laser system described, we find a basin boundary metamorphosis due to an inner tangency of a direct saddle followed by the disappearance of a chaotic attractor at a boundary crisis. The chaotic attractor is the closure of the unstable manifold of a flip saddle and this boundary crisis is due to a closure tangency involving this unstable manifold. The phenomenon of a closure tangency is typical in two-dimensional orientation-preserving diffeomorphisms and three-dimensional flows, as was demonstrated by identifying this type of boundary crisis in the Hénon map. At the boundary crisis the entropy associated with the chaotic attractor is positive, and it persists as the entropy associated with a chaotic saddle after the bifurcation.

Our computations of lower bounds on the entropy constitute a proof that the injection laser indeed displays chaotic dynamics. Apart from an interest in the laser community in applications of chaotic dynamics, for example, in communication schemes, this is also one of the first examples of a rigorous (computer assisted) proof of chaos in a technologically relevant physical system.

ACKNOWLEDGMENTS

The authors thank Hinke Osinga for valuable input concerning the literature on crisis bifurcations and Sebastian Wieczorek for helpful discussions. The research of P.C. was financially supported by the Leverhulme Trust and that of B.K. by an EPSRC ARF grant.

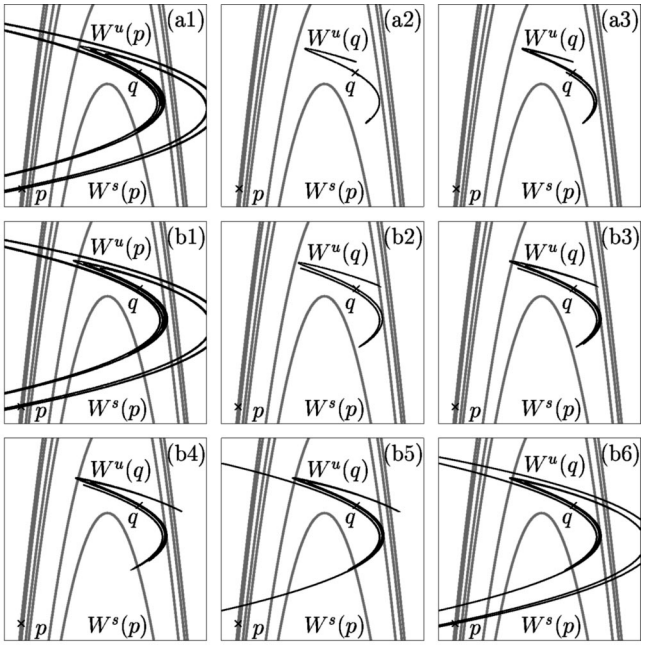

FIG. 7. The manifold $W^u(p)$ changes little in the closure tangency, see (a1) and (b1), but $W^u(q)$ changes dramatically. Before the closure tangency longer and longer pieces of $W^u(q)$ in panels (a2) and (a3) stay bounded, while after the closure tangency longer and longer pieces of $W^u(q)$ in panels (b2) to (b6) converge to $W^u(p)$. Close to the closure tangency one needs to compute very long pieces of $W^u(q)$ to see its convergence to $W^u(p)$; $b=0.5$, and $a=2.4$ (row a) and $a=2.5$ (rows b).

APPENDIX: CLOSURE TANGENCY IN THE HÉNON MAP

The scenario described above, in which a closure tangency is responsible for the destruction of a chaotic attractor, is typical in orientation-preserving diffeomorphisms, which include all return maps of flows. We describe here in more detail what this bifurcation means in terms of the stable and unstable manifolds of the saddles involved, because this is quite spectacular and not in the literature on boundary crises. Indeed, this bifurcation is responsible for the destruction of a chaotic attractor in the Hénon map

$$H(x,y)=H_{a,b}(x,y)=(a-x^2-by,x) \tag{A1}$$

in the orientation-preserving case $b>0$; see Ref. [40] for an example. We fix $b=0.5$, so H is uniformly dissipative, and vary the parameter a.

For sufficiently large a, H has two saddle fixed points, a direct saddle p and a is a flip saddle q, which means that we are in the same situation as discussed previously for the injected laser. For $a>0.840$ the manifolds $W^u(p)$ and $W^s(p)$ intersect transversely yielding homoclinic orbits to p. For parameter value $a=2.4$, $W^u(p)$ intersects both $W^s(p)$ and $W^s(q)$, but $W^u(q)$ does not intersect $W^s(p)$, as shown in Fig. 6(row a). The closure of $W^u(q)$ is a chaotic attractor A, and remains inside a region bounded by an arc of $W^u(p)$ and an arc of $W^s(p)$. The boundary of the basin of attraction of A is $\overline{W^s(p)}$.

For $a=2.5$, shown in Fig. 6(row b), the situation is very different. $W^u(q)$ now intersects $W^s(p)$. Since points which lie to the left of $W^s(p)$ escape to infinity, there is an open set in $\overline{W^u(q)}$ consisting of points which escape to infinity, and the set of points which escape is dense. The closure of the set of points heteroclinic to p and q is now a chaotic saddle, and gives only transient behavior of the map; all other points escape to infinity.

Once $W^s(p)$ and $W^u(q)$ intersect, they must do so arbitrarily close to p, and, by the Lambda Lemma [43], the closure of $W^u(p)$ contains $W^u(q)$. Hence, $W^u(p)$ and $W^u(q)$ have the same closures. This means that the branches of $W^u(q)$ now limits on the branch of $W^s(U)$ which extends to infinity. Hence, this type of boundary crisis is a discontinuity point of $\overline{W^u(q)}$ (using the Hausdorff metric on sets).

To illustrate this, in Fig. 7 we show how $W^u(q)$ is build up in successive iterates. In Figs. 7(a2) and 7(b2), we have computed $W^u(q)$ to length 1; successive figures are computed by iterating the unstable curve. Before the closure tangencies $W^u(q)$ remains bounded [Fig. 7(a3)]. After the closure tangency notice how for the first few iterates the unstable curve remains close to the former attractor [Fig. 7(b2)–(b4)], but, as higher iterates are computed, there are arcs that cross $W^s(p)$ closer and close to p [Fig. 7(b5)–(b6)]. Although the topology of the unstable manifold changes discontinuously at the limit bifurcation, for parameter values close to the induced boundary crisis, a very large number of iterates of the initial segment of unstable manifold are needed to cross a given arc in $W^s(p)$. This must be the case, since even though the topology of the manifold can change discontinuously, any fixed iterate must change continuously.

[1] E.N. Lorenz, J. Atmos. Sci. **20**, 130 (1963).

[2] J. Guckenheimer and P. Holmes, *Applied Mathematical Sciences, Nonlinear Oscillations, Dynamical Systems, and Bifurcations of Vector Fields* (Springer-Verlag, Berlin, 1983), Vol. 42.

[3] J.B. Pesin, Russ. Math. Surveys **32**, 55 (1977).

[4] P. Grassberger, *Chaos* (Manchester University Press, Manchester, 1986), p. 291.

[5] P. Cvitanović, G.H. Gunaratne, and I. Procaccia Phys. Rev. A **38**, 1503 (1988).

[6] P. Grassberger and H. Kantz, Phys. Lett. **113A**, 235 (1985).

[7] F. Christiansen and A. Politi, Phys. Rev. E **51**, 3811 (1995).

[8] F. Christiansen and A. Politi, Nonlinearity **9**, 1623 (1996).

[9] F.A. McRobie and J.M.T. Thompson, Dyn. Stab. Syst. **9**, 223 (1994).

[10] V. Rom-Kedar, Nonlinearity **7**, 441 (1994).

[11] K. Mischaikow, in *Dynamical Systems*, edited by R. Johnson, Lecture Notes In Mathematics Vol. 1609 (Springer-Verlag, Berlin, 1997), pp. 119.

[12] A. Szymczak, Fund. Math. **148**, 71 (1995).

[13] P. Collins Int. J. Bifurcation Chaos Appl. Sci. Eng. **12**, 605 (2002).

[14] P. Collins, in *Geometry and Topology in Dynamics*, edited by M. Barge and K. Kuperberg, Contemporary Mathematics Vol. 246 (American Mathematical Society, Providence, 1999).

[15] R. Bowen, in *Global Analysis, Proceedings of Symposia in Pure Mathematics* (American Mathematical Society, Providence, RI, 1970), Vol. 14, p. 23.

[16] M. Misiurewicz, Astérisque **40**, 147 (1976).

[17] R.L. Davidchack and Y.-C. Lai, Phys. Rev. E **60**, 6172 (1999).

[18] L.A. Lugiato, L.M. Narducci, D.K. Bandy, and C.A. Pennise, Opt. Commun. **46**, 64 (1983).

[19] J.R. Tredicce, F.T. Arecchi, G.L. Lippi, and G. Puccioni, J. Opt. Soc. Am. B **2**, 173 (1985).

[20] V. Kovanis, A. Gavrielides, T. Simpson, and J. Liu, Appl. Phys. Lett. **67**, 2780 (1995).

[21] T.B. Simpson, J.M. Liu, K.F. Huang, and K. Tai, Quantum Semiclassic. Opt. **9**, 765 (1997).

[22] S.M. Wieczorek, B. Krauskopf, and D. Lenstra, Opt. Commun. **172**, 279 (1999).

[23] S.M. Wieczorek, B. Krauskopf, and D. Lenstra, Phys. Rev. E **64**, 056204 (2001).

[24] V. Annovazzi-Lodi, S. Donati, and A. Scire, IEEE J. Quantum Electron. **32**, 953 (1996).

[25] H.F. Chen and J.M. Liu, IEEE J. Quantum Electron. **36**, 27 (2000).

[26] S. Wieczorek, T.B. Simpson, B. Krauskopf, and D. Lenstra, Phys. Rev. E **65**, 045207 (2002).

[27] B. Krauskopf, S.M. Wieczorek, and D. Lenstra, Appl. Phys. Lett. **77**, 1611 (2000).

[28] S.M. Wieczorek, B. Krauskopf, and D. Lenstra, Opt. Lett. **26**, 816 (2001).

[29] C. Grebogi, E. Ott, and J.A. Yorke, Physica D **7**, 181 (1983).

[30] C. Grebogi, E. Ott, and J.A. Yorke, Phys. Rev. Lett. **56**, 1011 (1986).

[31] C. Grebogi, E. Ott, and J.A. Yorke, Physica D **7**, 243 (1987).

[32] C. Robert, K.T. Alligood, E. Ott, and J.A. Yorke, Physica D **144**, 44 (2000).

[33] H. Osinga and U. Feudel, Physica D **141**, 54 (2000).

[34] X.-S. Yang, Chaos, Solitons Fractals **11**, 2157 (2000).

[35] M. Hénon, Commun. Math. Phys. **50**, 69 (1976).

[36] K. Ikeda, Opt. Commun. **30**, 257 (1979).

[37] B. Krauskopf and H. Osinga, J. Comput. Phys. **146**, 404 (1998).

[38] H. Osinga, Int. J. Bifurcation Chaos Appl. Sci. Eng. (to be published).

[39] E.J. Doedel, A.R. Champneys, T.F. Fairgrieve, Yuri A. Kuznetsov, B. Sandstede, and X.J. Wang, AUTO97: Continuation and bifurcation software for ordinary differential equations (http://indy.cs.concordia.ca/auto/).

[40] J. Gallas, C. Grebogi, and J.A. Yorke, Phys. Rev. Lett. **71**, 1359 (1993).

[41] S.E. Newhouse, *Dynamical Systems*, CIME Summer School, Bressanone, 1979, Progress in Mathematics Vol. 8 (Birkhäuser, Boston, 1980), pp. 1–114.

[42] J. Palis and F. Takens, *Hyperbolicity and Sensitive Chaotic Dynamics at Homoclinic Bifurcations*, Cambridge Studies in Advanced Mathematics Vol. 35 (Cambridge University Press, Cambridge, UK, 1993).

[43] J. Palis, Topology **8**, 385 (1969).